The Effect of Relative Permeability Hysteresis on the Design of an Optimal Water-Alternating-Gas (WAG) Process

M. Kowsari; L. A. James; and R. D. Haynes, Memorial University of Newfoundland

Corresponding Author: L. A. James
E-mail: ljames@mun.ca

Abstract

Water-alternating-gas (WAG) as a tertiary recovery method is applied to oil reservoirs at a later stage of reservoir life to more or less success depending on field and operation. Uncertainty in WAG optimization has been shown to be dependent on several factors including reservoir characterization, WAG timing, and its operation. This paper comprehensively explores WAG optimization in the context of WAG operating parameters and hysteresis, the first paper to explore both simultaneously. WAG operating parameters have been analyzed and optimized at both the core and field scale with a general conclusion that the timing, miscibility, WAG ratio, cycle time, and number of cycles play a varying role in the WAG optimization. Reservoir characterization has considered well configuration, oil type, rock properties, and hysteresis in relative permeability. The cyclic nature of WAG and the dependency of the relative permeability on the saturation history, the relative permeability hysteresis modeling plays a key role in WAG performance where different hysteresis models will predict different results, as shown in literature. This paper considers the choice of hysteresis model and WAG operating parameters on WAG optimization. First, a sensitivity analysis is performed to evaluate the effect of hysteresis models (no hysteresis, Carlson, and Killough) on a large number of WAG development scenarios sampled by the Latin Hypercube Sampling method. Next, optimizations were conducted to compare and analyze the optimum recovery factor and corresponding optimal WAG operating parameters for various combinations of hysteresis models. The results of the study indicate that excluding hysteresis modeling from simulations would likely lead to a higher predicted produced volume of the non-wetting phases, i.e. oil and gas, and a lower predicted produced volume of the wetting phase, i.e. water. Also, the optimal recovery factor as well as the optimal WAG operating parameters can be significantly affected by the choice of the hysteresis models.

Introduction

Water-alternating-gas (WAG) as a tertiary recovery method is traditionally applied to oil reservoirs at a later stage of reservoir life, following a secondary water or gas injection. The decision whether or not to employ an enhanced oil recovery (EOR) method is based on specialized core analysis, economic analysis, and simulation and optimization studies. Decisions are made during the intermediate stage of the fields' production life after a considerable amount of production data is collected and reservoir simulation models are matched accordingly. Production data is used to history match the reservoir model by tuning reservoir geological properties such as the permeability and porosity distributions. In addition, the collected data can be used to reduce uncertainty in two-phase relative permeability data, particularly when gas or water is injected. During primary and secondary production stages, the direction of saturation changes is generally toward reducing oil saturation and increasing the saturation of the other phase (either gas or water). Therefore, the production data gives no insight with respect to the hysteresis effect which refers to the path and the history dependency of relative permeability curves. Severals studies [Vivek and Suresh Kumar (2019); Spiteri et al. (2008); Guzman et al. (1994)] have shown that the relative permeability hysteresis can significantly affect the recovery in a WAG process. History-dependent saturation modeling has an important role in the numerical simulation of WAG recovery. It has been shown that in order to accurately model WAG injection, the hysteresis effect must be considered. Two comparative studies on hysteresis modeling [Hoseini et al. (2011); Hamzei et al. (2011)] indicate that the results of WAG simulation utilizing a commercial simulator can be misleading if hysteresis modeling is not properly applied. They illustrated the effect of choosing different hysteresis models on WAG performance using a simple synthetic model and a more complex heterogeneous reservoir model. Their investigation was, however, limited to a single WAG development scenario. It is unclear how the production profiles would look when more WAG development scenarios are simulated. The production of all three phases (oil, water, and gas) for numerous WAG development scenarios were analyzed in order to determine a statistically meaningful conclusion.

Chen and Reynolds (2016) demonstrated that a sub-optimal design of WAG can result in poor recovery. Therefore, WAG optimization is necessary to achieve the optimal recovery in a development scenario. Several studies [You et al. (2019); Kengessova (2020); Mohagheghian et al. (2018); Bahagio (2013); Chen

et al. (2010); Johns et al. (2003); Mirkalaei et al. (2011); Zhou et al. (2012); Ghaderi et al. (2012); Bender and Yilmaz (2014)] have proposed various optimization methods to design an optimal WAG development scenario. However, these studies assumed a single hysteresis model in the reservoir model. The effect of the hysteresis modeling on the optimal WAG development has not been investigated or included in the aforementioned WAG optimization literature. It is unknown how the choice of the hysteresis model can affect the value of the optimal recovery factor and/or whether the inclusion of hysteresis will affect the optimal development scenario. It is important to understand how the lack of hysteresis modeling or the specific choice of hysteresis can affect the optimal WAG design.

The contribution of this study is that it investigates the effect of the choice of relative permeability hysteresis model on the design of WAG injection (optimization of WAG operating parameters). Previous WAG optimization considered either hysteresis or WAG operating parameters, not both. Specifically, the following questions are considered.

1. How sensitive are the simulation results, such as ultimate recovery, produced water, and produced gas, to the choice of relative permeability hysteresis model?

2. What is the effect of the choice of relative permeability hysteresis model on the **optimal** recovery factor?

3. Will the relative permeability hysteresis model affect the **optimal** WAG operating parameters?

The goal of this paper is to comprehensively investigate the uncertainty of hysteresis model (no hysteresis, Carlson, or Killough) on WAG optimization considering multivariable (WAG timing, injection rate, cycle time, slug size) stochastic optimization methods. The goal of this paper is NOT to find a single correct hysteresis model but to explore how relative permeability hysteresis may impact WAG optimization.

Materials and Methods

Relative Permeability Hysteresis Models. The relative permeability depends on the fluid saturations, the saturation path and saturation history. As depicted in Figure 1, assuming a water-wet porous media, the relative permeability values for a drainage process (increasing oil saturation) are different from that of an imbibition process (increasing water saturation). This phenomenon is called the hysteresis effect in relative permeability.

Carlson Models. In the Carlson (1981) model, the scanning curves are assumed to be parallel to the imbibition curve, as shown in Figure 1. The curves are simply produced by shifting the imbibition curve from the saturation reversing point until it intersects the drainage curve. The Carlson model can only be applied to the non-wetting phase.The Carlson relative permeability can be calculated from

$$K_{rn}\left(S_n\right) = K_{rni}(S_n - S_{ns}),$$

where

$$S_{ns} = S_{hy} - S_{ni}(K_{rn}(S_{hy}))$$

and S_{hy} is the maximum non-wetting phase saturation reached.

Killough Model. Killough model provides a method to generate smooth scanning curves between drainage and imbibition.The Killough model can be applied to both the non-wetting and wetting phases.

Non-wetting phase. The Killough (1976) model requires the calculation of the trapped critical saturation that can be found from

$$S_{ncrt} = S_{ncrd} + \frac{S_{hy} - S_{ncrd}}{1 + C(S_{hy} - S_{ncrd})}.$$

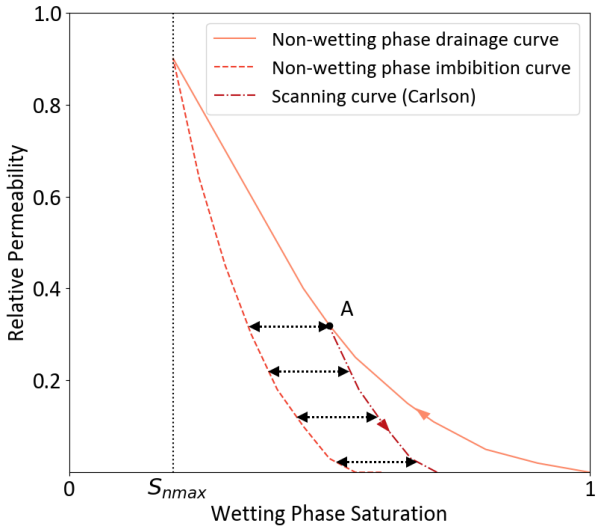

Fig. 1 – Demonstration of parallel scanning curve obtained by the Carlson hysteresis model.

Here, C is called Land's trapping parameter and can be computed as follows:

$$C = \frac{1}{S_{ncri} - S_{ncrd}} - \frac{1}{S_{n\ max} - S_{ncrd}},$$

where S_{ncrt} is the non-wetting phase trapped critical saturation and S_{nmax} is maximum saturation of the non-wetting phase. S_{hy} is the maximum non-wetting phase saturation reached. The non-wetting phase critical saturation from the drainage curve and the non-wetting phase critical saturation from the imbibition curve are represented by S_{ncrd} and S_{ncri}, respectively. The saturation parameters, S_{ncri}, S_{hy}, S_{ncrd}, S_{nmax}, and S_{ncrt}, are illustrated graphically in Figure 2.

Given a set of non-wetting phase drainage and imbibition curves, K_{rnd} and K_{rni}, the hysteresis dependent relative permeability of the non-wetting phase K_{rn} can be calculated from

$$K_{rn}\left(S_n\right) = \frac{K_{rni}(S_{norm})K_{rnd}(S_{hy})}{K_{rnd}(S_{n\,\max})},$$

where,

$$S_{norm} = S_{ncri} + \frac{\left(S_n - S_{ncrt}\right)\left(S_{n\ max} - S_{ncri}\right)}{S_{hy} - S_{ncrt}}.$$

Wetting phase. As described in the Eclipse Documentation Schlumberger (2017), the Killough model implemented in the simulator uses some of the saturation parameters introduced above (in the non-wetting phase). The wetting phase relative permeability K_{rw} at saturation of $1 - S_{ncrt}$ is given by

$$K_{rw}(1 - S_{ncrt}) = K_{rwd}(1 - S_{ncrt}) + [K_{rwi}(1 - S_{scri}) - K_{rwd}(1 - S_{ncri})](\frac{S_{ncrt} - S_{ncrd}}{S_{ncri} - S_{ncrd}}),$$

where K_{rwd} and K_{rwi} are the values of the bounding drainage and imbibition relative permeability curves, respectively. Given a wetting phase saturation of S_w the relative permeability on the scanning curve is calculated as

$$K_{rw}(S_w) = K_{rwd}(1 - S_{hy}) + \frac{[K_{rw}(1 - S_{ncrt}) - K_{rwd}(1 - S_{hy})]K_{rwi}(1 - S_{norm})}{K_{rwi}(1 - S_{ncri}).}$$

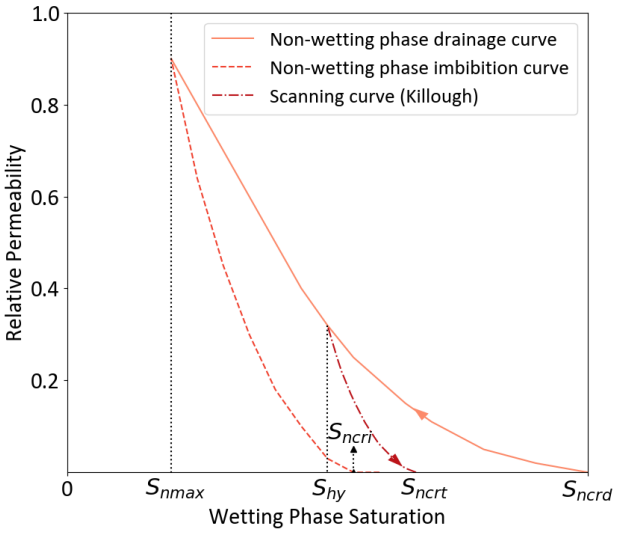

Fig. 2 – Demonstration of saturation parameters in the Killough hysteresis model.

Sensitivity Analysis. A sensitivity analysis was designed to investigate the effect of hysteresis models on total produced oil, total produced water, and total produced gas. The sensitivity analysis includes running numerous WAG development scenarios using each hysteresis case. Latin Hypercube Sampling (LHS) was used to generate the sample development scenarios for both reservoir models. LHS, introduced by McKay et al. (1979), is a stratified Monte Carlo sampling method for evaluating the expectation of outputs in computer simulations. For the simple SPE-5 model, a total of 5,000 development scenarios were created. The PUNQ-S3 was tested using 10,000 development scenarios due to the high complexity. For each hysteresis model, as defined in Table 7, all of the sampled WAG development scenarios are run using the Eclipse simulator and the total produced oil, total produced water, and total produced gas were recorded. As the purpose of the sensitivity analysis was to understand the effect of the choice of hysteresis model, not the effect of the WAG development scenarios, the results of each run were normalized with respect to the results obtained from case 0. Normalizing the parameters eliminated the effect of the WAG development scenario while maintaining the effects of the hysteresis model itself. Given the development scenario n, and hysteresis case i, the normalized parameter, $P^i_{norm,n}$, is calculated as

$$P^i_{norm,n} = \frac{P^i_n}{P^0_n},$$

where P^i_n is the value of the parameter using hysteresis case i (e.g. P^5_n is the total produced oil obtained using the Killough model for all of three phases and running the simulation under the development scenario n), and P^0_n is the value of the parameter obtained by using the no hysteresis model and running under the same development scenario, n.

Optimization Framework. The objective function used for this study is the incremental oil recovery, U, defined by

$$U = RF_{WAG} - RF_{WF},$$

where RF_{WAG} is the oil recovery obtained by implementing a WAG process and RF_{WF} is the oil recovery obtained by an optimal water flood scenario. The recovery factor is calculated by the following equation.

$$RF = \frac{N_p}{OOIP},$$

where N_p is the produced oil in standard condition and $OOIP$ is the original oil in place. For each hysteresis case, c_j, as defined in Table 7, the optimization problem considered is

$$\begin{aligned} \max \quad & U = f(x, c_j) \\ \text{s.t.} \quad & a_i < x_i < b_i \end{aligned}$$

where x is our optimization variable that includes the start time of the WAG, the gas and water cycle lengths, and the water and gas injection (guide) rates for each injector. The cycle length also determines the mode of the injector which can be set as WAG (water and gas injection), water injection only, or gas injection only. The injection guide rates were selected as optimization variables rather than the WAG slug sizes. Specifying the exact WAG ratio was not practical due to the constraints imposed by the simulator, such as the fracture pressure and voidage replacement ratio. Injection rates were optimized for the SPE-5 model, whereas injection guide rates were optimized for the PUNQ-S3 model. Using injection guide rate control, the total target injection rate, which is governed by the voidage replacement ratio, is divided between all the injectors in proportion to the specified "guide" rates. This setup makes it possible to inject only a single phase in one or more injectors while having WAG injection in the other injectors. The bounds of the variables, a_i and b_i, are shown in Tables 1 and 2. The WAG start time is defined as the time when the waterflooding stops and WAG injection starts. The range of this variable is set such that the optimization algorithm decides whether or not to implement a WAG scenario and when to start the WAG process.

Variable	Min. Value	Max.Value	No. of Variables
WAG Initiation Time (years)	0	18 (1 PV)	1
Water Injection Rate (Rm^3)	1,000	8,000	1
Gas Injection Rate (Rm^3)	1,000	8,000	1
Water Cycle Length	gas injection	1095 days	1
Gas Cycle Length	water injection	1095 days	1

Table 1 – The range of optimization variables for the SPE-5 model

Variable	Min. Value	Max.Value	No. of Variables
WAG Initiation Time (years)	0	40 (1 PV)	1
Water Injection Guide Rate	10	100	4*
Gas Injection Guide Rate	10	100	4*
Water Cycle Length	gas injection	1095 days	4*
Gas Cycle Length	water injection	1095 days	4*

Table 2 – The range of optimization variables for the PUNQ-S3 model (*one per injector)

Two stochastic population-based optimization algorithms were used to solve the optimization problems: Particle Swarm Optimization (PSO) Kennedy and Eberhart (1995) and Evolutionary Strategy (ES) Beyer and Schwefel (2002). These methods are selected as they have been used with success in production optimization problems [Mohagheghian et al. (2018); Jesmani et al. (2016); Humphries and Haynes (2015); Humphries et al. (2014); Wang et al. (2016); Bouzarkouna et al. (2012); Forouzanfar et al. (2015)]. The key advantages of these methods are that; i) they are derivative-free and non-invasive; and ii) they are population-based hence can be parallelized easily. The PSO algorithm searches the solution domain via a swarm of particles in each iteration. Each particle represents a solution to the optimization problem. The location of the particles (x) updates in each iteration (t) by the magnitude of the velocity (v) of each particle which is determined by its previous best (p_b) and the global best (g_b).

$$(x_t) = x_{t-1} + v_t,$$

where v_t is calculated by the following equation

$$(v_t) = v_{t-1} + \Phi_p(p_b - x_{t-1}) + \Phi_g(g_b - x_{t-1}),$$

where Φ_p and Φ_g are the weights for particle best and global best, respectively. The weights are chosen randomly for each particle in every iteration from a uniform distribution. The flowchart of the PSO algorithm is shown in Figure 3.

The implementation of the PSO in our study is based on the algorithm as presented in Poli et al. (2007). The parameter settings of the PSO algorithm are shown in Table 3.

Parameter	SPE-5	PUNQ-S3
Initial Population	Random	Random
Number of Generations	40	40
Population Size	125	250
Maximum Function Evaluations	5,000	10,000
Population Best WeightΦ_p	2.0	2.0
Global Best WeightΦ_g	2.0	2.0

Table 3 – Particle Swarm Optimization algorithm parameter settings

ES is a sub-class of nature-inspired optimization algorithms belonging to the class of Evolutionary Algorithms. These types of optimization algorithms utilize recombination, mutation, and selection applied to a population of individuals containing candidate solutions in order to evolve iteratively toward the optimal solution. ES is designed for numerical optimization of non-linear or non-convex continuous optimization problems. The unique feature of the ES algorithm is that the mutation strength is subject to evolution similar to the optimization variables. The flowchart shown in Figure 4 summarizes the steps used in the algorithm. More detailed explanation of the algorithm is discussed in Beyer and Schwefel (2002). Table 4 shows the parameter settings of the implementation of the ES for this study. The Distributed Evolutionary Algorithm in Python (DEAP) library, Fortin et al. (2012), was used to implement both optimization algorithms.

Parameter	SPE-5	PUNQ-S3
Initial Population	Random	Random
Number of Generations	40	40
Population Size	60	100
Number of Offspring	120	250
Maximum Function Evaluations	5,000	10,000
Mutation Rate	0.3	0.3
Crossover Rate	0.7	0.7
Crossover Method	BLX-α	BLX-α
Mutation Method	Uncorr. n-step size	Uncorr. n-step size
Survivor Selection Method	(μ, λ)	(μ, λ)
Parent Selection Method	Uniform (random)	Uniform (random)

Table 4 – Evolution Strategy algorithm parameter settings

The optimization experiments were repeated three times (three trials) as both algorithms are stochastic in nature and it is possible that the global best will not be found with only one attempt. Each trial consisted of 5,000 function evaluations (simulation runs) for the SPE-5 model and 10,000 function evaluations for the PUNQ-S3 model.

Reservoir Models. Two compositional reservoir models used for the simulation studies, the PUNQ-S3 and SPE-5, are briefly described next.

SPE-5 Benchmark. The modified SPE-5 benchmark reservoir model was chosen as a simple and homogeneous model which was used in a WAG study by Killough and Kossack (1987). The porosity of the reservoir is 30%, which produces a pore volume of 10.56 M Rm^3. The initial oil in place is 8.45 M Rm^3 (6.76 M Sm^3) and the initial oil saturation is 80%. The model contains 147 ($7 \times 7 \times 3$) grid blocks. It has one producer

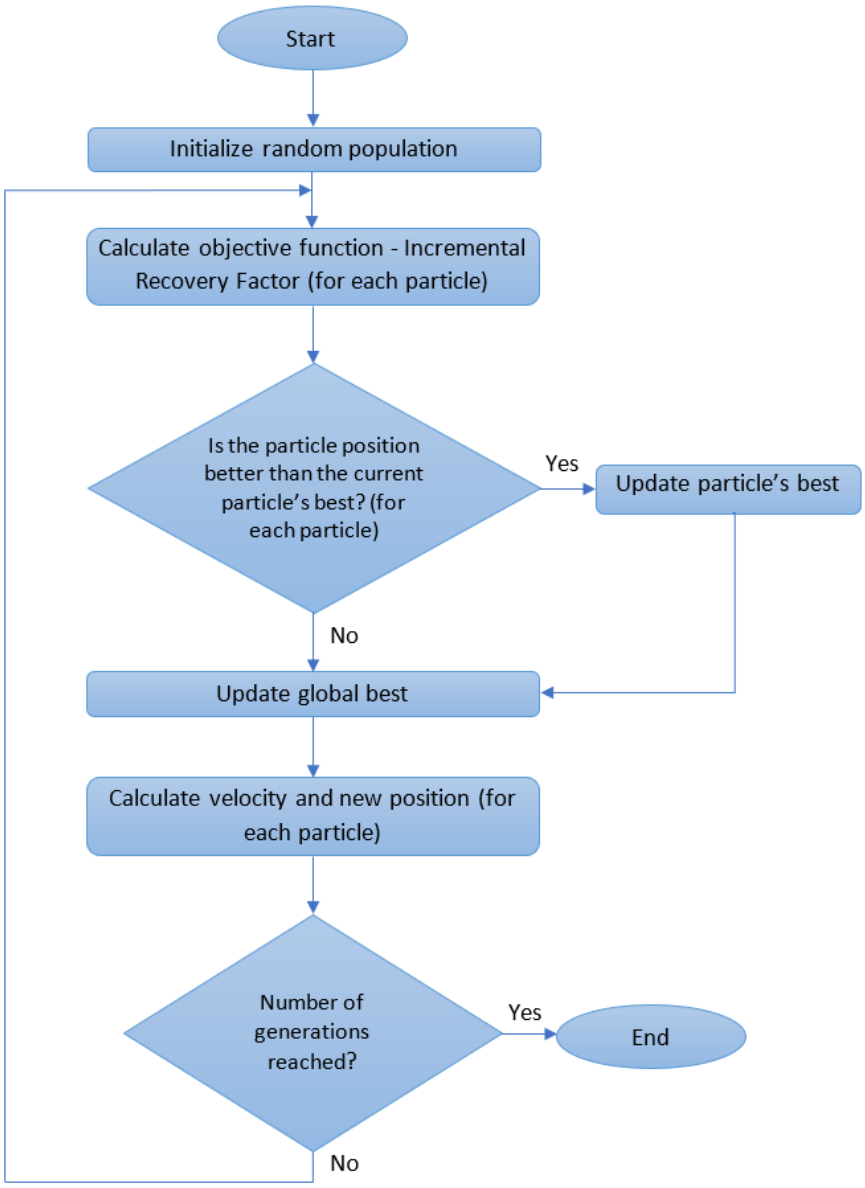

Fig. 3 – Particle Swarm Optimization Flowchart

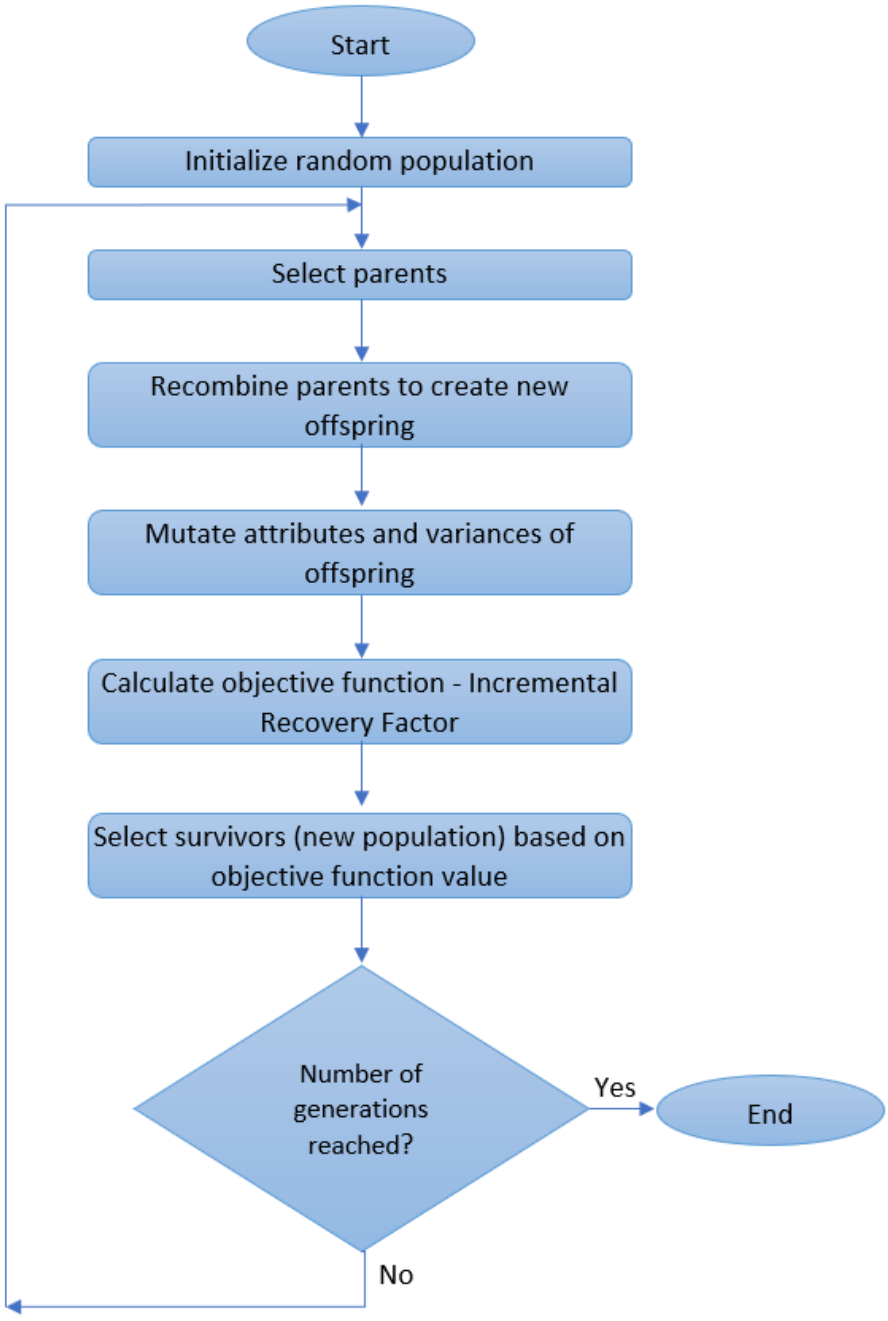

Fig. 4 – Evolutionary Strategy Flowchart

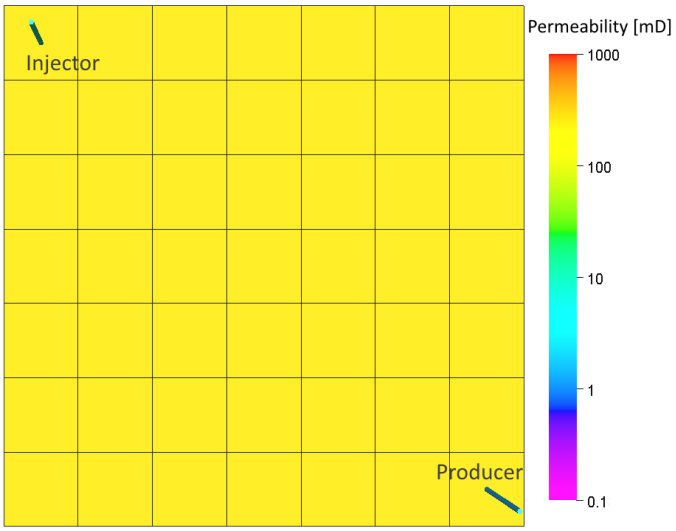

Fig. 5 – Modified SPE-5 Benchmark

and one injector. The locations of these wells and the permeability of the top layer are shown in Figure 5. The drainage and imbibition relative permeability curves used in simulations are shown in Figures 6 and 7. The composition of the oil and injection gas phases are provided in Table 5.

Component	Oil Phase	Injection Gas
C1	0.50	1.0
C3	0.03	0.0
C6	0.07	0.0
C10	0.20	0.0
C15	0.15	0.0
C20	0.05	0.0

Table 5 – Fluid Compositions in SPE-5 Model

PUNQ-S3. The second reservoir model chosen for this study is the PUNQ-S3 benchmark, which is a more complex and heterogeneous reservoir model. It is based on a field example provided by Elf Exploration Production (Floris et al. (2001)). The model contains a total of 2660 grid blocks with the dimensions of $19 \times 28 \times 5$ of which 1761 blocks are active. The reservoir contains a small gas cap located in the center of the dome shaped structure. The total pore volume of the reservoir is 35.36 M Rm^3. The total volume of the original oil in place is 17.37 M Sm^3. The original model has a non-injection development scheme and produces from six wells. The development scheme was modified to make WAG injection possible by adapting an injection scheme similar to Spiteri and Juanes (2006), where two of the producers were removed and four injectors were introduced. Figure 8 shows the permeability of the top layer and the location of the injectors and producers.

The drainage and imbibition relative permeability curves used in simulations are shown in Figures 9 and 10. The composition and the properties of the oil and injection gas phases are provided in Table 6.

The Eclipse reservoir simulator provides six two-phase hysteresis options. Each case, as defined in Table 7, represents a hysteresis option in the simulator. Case 0 is the base case, which does not incorporate hysteresis (only drainage curves are used).

Results

Sensitivity Analysis. A sensitivity analysis was conducted to compare the total produced oil, total produced gas, and total produced water with all hysteresis cases under various WAG development scenarios. Results

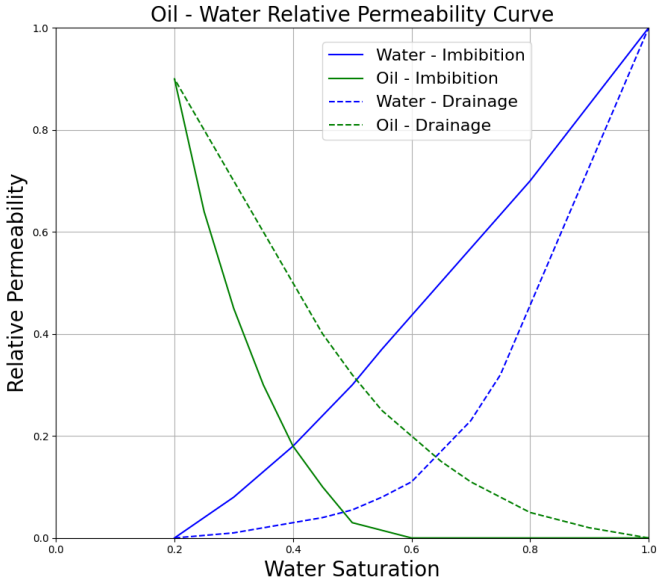

Fig. 6 – SPE-5 Water - Oil Relative Permeability Curves

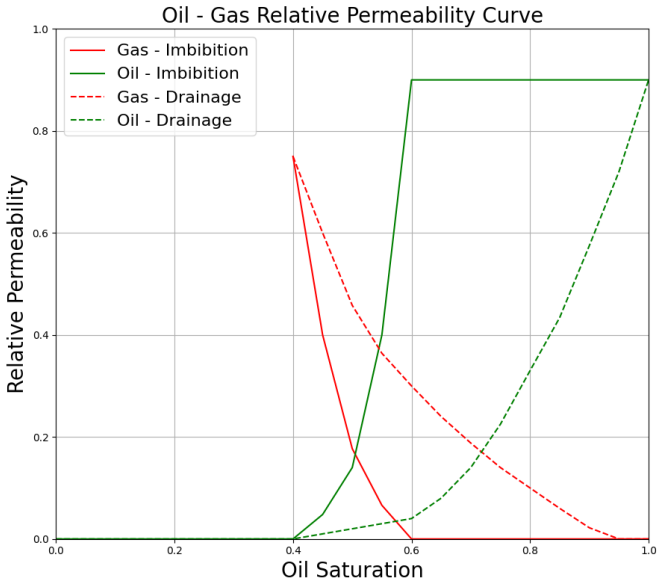

Fig. 7 – SPE-5 Gas - Oil Relative Permeability Curves

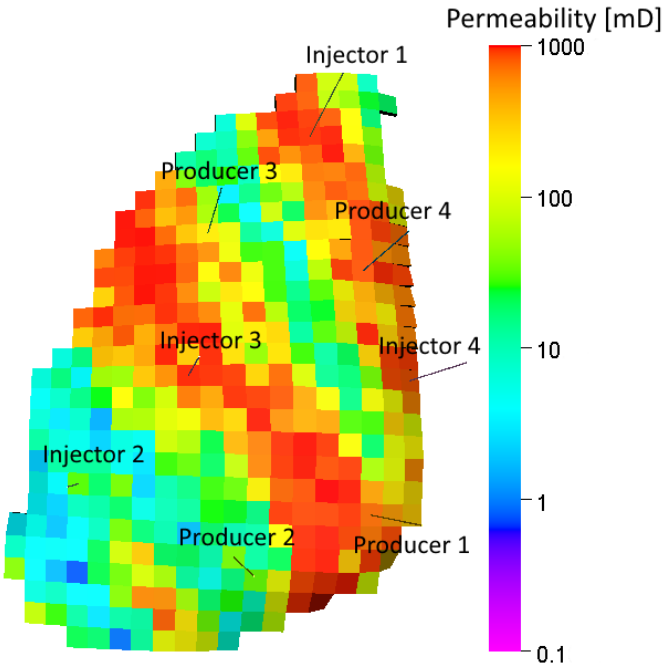

Fig. 8 – Modified development scheme used in PUNQ-S3 model

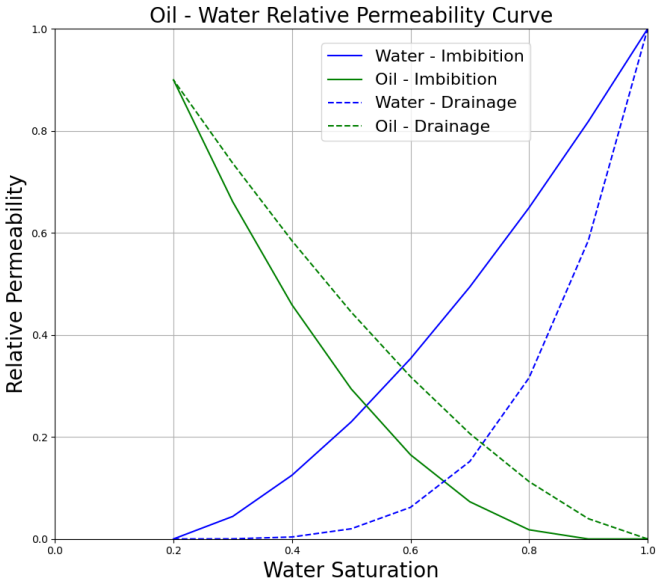

Fig. 9 – PUNQ-S3 Water - Oil Relative Permeability Curves

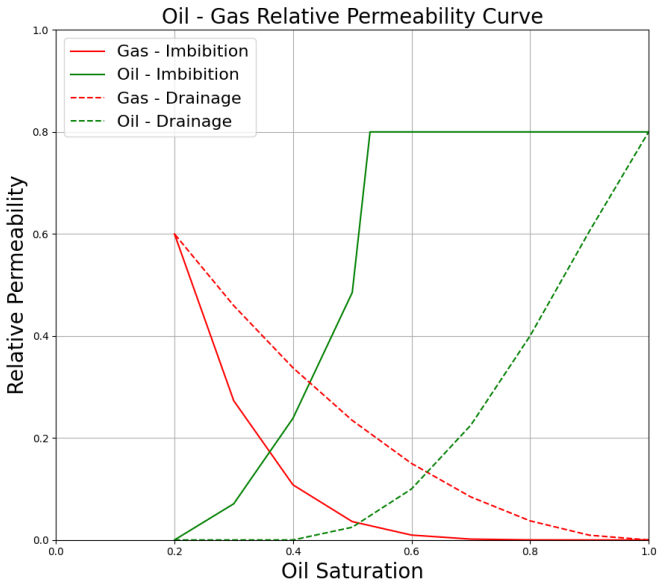

Fig. 10 – PUNQ-S3 Gas - Oil Relative Permeability Curves

Component	Oil Phase	Injection Gas
C1	0.43	1.0
C3	0.03	0.0
C6	0.06	0.0
C10	0.24	0.0
C15	0.18	0.0
C20	0.06	0.0

Table 6 – Fluid Compositions in PUNQ-S3 Model

are illustrated in Figures 11-13. Each bar in Figures 11 represents the mean normalized total produced oil for all the development scenarios and is calculated as

$$P^i_{avg} = \frac{\sum_{n=1}^{N} P^i_{norm,n}}{N},$$

where $P^i_{norm,n}$ is the total produced oil normalized with respect to the no hysteresis case (case 0) and N is the total number of development scenarios (5,000 for SPE-5 and 10,000 for PUNQ-S3). The error bars show the standard deviation of the normalized total produced oil, calculated as

$$P^i_{err} = \sqrt{\frac{\sum_{n=1}^{N} |P^i_{avg} - P_{norm,n}|}{N}}.$$

As shown, on average, using only the drainage curves, i.e. no hysteresis model, predicts the highest ultimate oil recovery. The results also show that between the cases with an active hysteresis option, the predicted oil recovery is reservoir model-dependent. For instance, while case 1 (Carlson model for gas and oil phases and the drainage curve for the water phase) has the highest predicted oil recovery when used in the PUNQ-S3 model, it predicts a relatively low oil recovery when used in the SPE-5 model. Comparing the values of the normalized total produced oil between the two reservoir models, one can observe that the deviation from the no hysteresis model is less for the more complex model (i.e. PUNQ-S3).

Figure 12 and Figure 13 illustrate the hysteresis model effect on the total produced water and total produced gas, respectively. The calculations of the bars and the error bars are similar to that of the total produced oil.

Case No.	Gas and Oil Hysteresis Model	Water Hysteresis Model
0	Drainage Curve	Drainage Curve
1	Carlson	Drainage Curve
2	Carlson	Imbibition Curve
3	Killough	Drainage Curve
4	Killough	Imbibition Curve
5	Killough	Killough

Table 7 – The hysteresis cases as used for optimization and sensitivity analysis

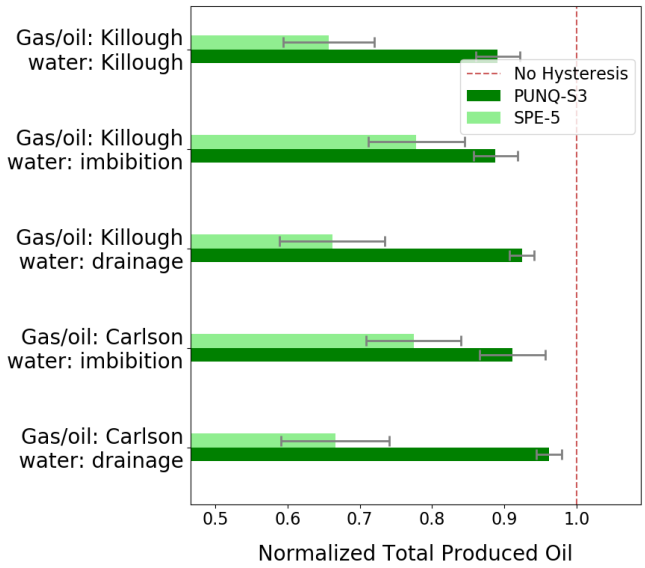

Fig. 11 – Sensitivity of total produced oil to the choice of hysteresis model

The results indicate that using the Killough model or the imbibition curve (hysteresis cases 2, 4, and 5) for the water phase would result in a higher predicted value of total produced water. However, when the drainage curve is used (case 1 and 3) the predicted value is smaller and it is even lower than the no hysteresis case for the SPE-5 model. Similar to the result of the oil phase, the deviation of the total produced water from the no hysteresis model is less for the more complex model (i.e. PUNQ-S3). As shown in Figure 13, the predicted value of produced gas is lower when a hysteresis model is active. However, within the cases with active hysteresis, the predicted value of total produced gas seems to be model-dependent. Similar to the oil phase, it appears the reservoir model properties have a significant effect on the extent that hysteresis models impact the produced volume of gas. Comparing Figures 11, 12, and 13, generally we can expect a higher produced volume of the wetting phase, water, and a lower produced volume of the non-wetting phases, oil and gas, when the hysteresis option is active for that phase. Also, it can be observed that there is more deviation from the no hysteresis case in the SPE-5 model. This is consistently true for all three parameters, the total produced oil, total produced gas, and total produced water. We believe the higher heterogeneity and complexity in the PUNQ-S3 model, which causes earlier water and gas breakthrough, have a greater influence on the production of the phases and dominate the hysteresis effects. Therefore, the heterogeneity of the PUNQ-S3 model appears to be contributing to dampening the effect of the hysteresis model.

Optimization.

Incremental Recovery Factor. WAG development scenarios are often compared to a base case water flooding scenario. It is assumed that this waterflood scenario will be the base development scenario if WAG is not

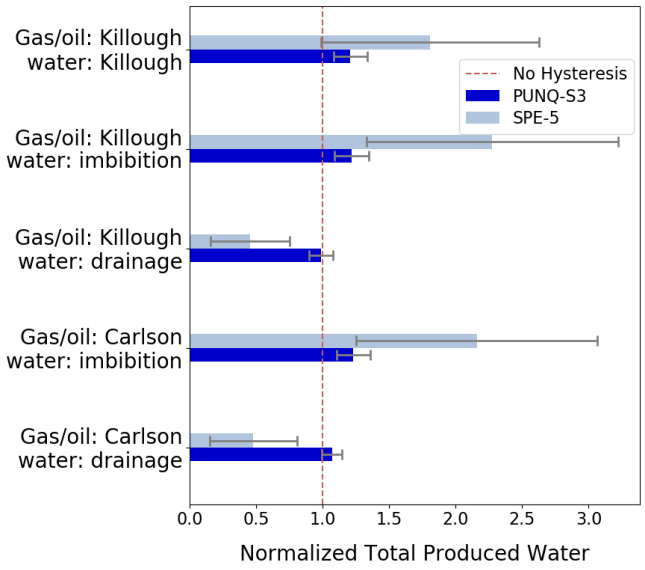

Fig. 12 – Sensitivity of total produced water to the choice of hysteresis model

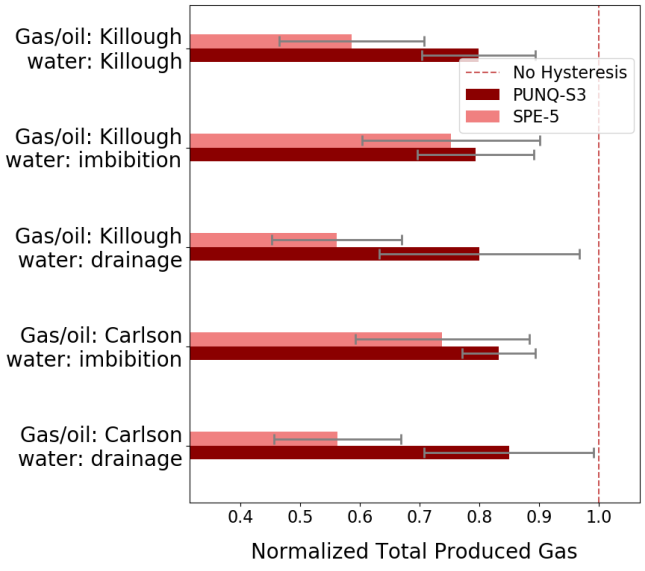

Fig. 13 – Sensitivity of total produced gas to the choice of hysteresis model

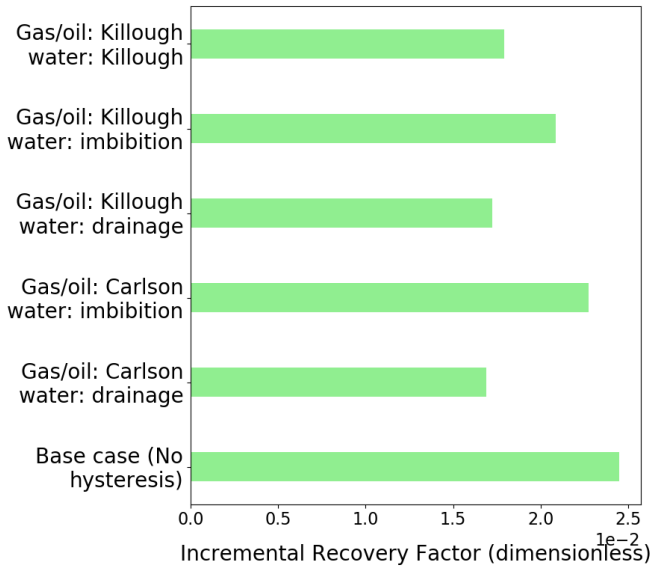

Fig. 14 – Optimal Incremental Recovery Factor (SPE-5)

implemented. Therefore, prior to performing WAG optimization, a base case was established by optimizing the waterflood scenario. The amount of oil produced by the optimal waterflooding scenario was 5.02 M Sm^3 for the SPE-5 model and 11.14 M Sm^3 for the PUNQ-S3. These are equivalent to recovery factors of 74.3% and 64.3%, respectively. Implementing WAG in most cases is only desirable if incremental oil to the optimal waterflooding can be produced.

For each reservoir model, the optimization algorithms, PSO and ES, were used to find the optimal development WAG scenario. Each optimization algorithm was tried three times for each hysteresis case, therefore, we have the results of 6 optimization trials for each hysteresis case. The results presented in this paper reflect the best of these 6 trials. Figure 14 and 15 illustrate the optimal recovery factor of the SPE-5 and PUNQ-S3 for each hysteresis case. For the SPE-5 model, the no hysteresis case predicts the highest incremental recovery. However, using the Carlson model for the gas and oil phases and drainage curve for the water phase (case 1) and using the Killough model for the gas and oil phases and drainage curve for the water phase (case 3) predict the lowest optimal recovery factor. This prediction is consistent with the results of sensitivity analysis on the total produced oil (Figure 11). In contrast to the SPE-5 results, the optimal recovery factor of the PUNQ-S3 model does not agree with the sensitivity analysis results. Figure 15 shows the optimal incremental recovery results using the PUNQ-S3 model. As illustrated, when the Carlson model was used for the gas and oil phases and the drainage curve used for the water phase (case 2), the optimal WAG scenario is the most optimistic with an incremental recovery factor of 17.5%. Case 3 shows only 9.1% improvement from the optimal water flood scenario. The difference between the two cases is 8.4%, which is equivalent to 1.46 M Sm^3 of oil. The results of WAG optimization on both reservoir models indicate that the optimal recovery factor value is a function of the hysteresis model. For instance, for the PUNQ-S3 reservoir model, assuming that WAG is only justified when the incremental recovery factor is above 10%, a decision-maker may discard WAG as an EOR option if case 3 was selected as the hysteresis model. The decision is correct only if the decision-maker is confident that the hysteresis behavior of the reservoir is best modeled by the case 3 hysteresis model. The dependency of the optimal WAG development scenario on the choice of the hysteresis model is discussed in the next section.

Optimal Development Scenarios. The optimal time to start the WAG injection for the SPE-5 model is shown in Figure 16. When no hysteresis model is used, the optimal recovery is achieved by a late WAG implementation. An early start is required when applying any hysteresis models, ideally within the first

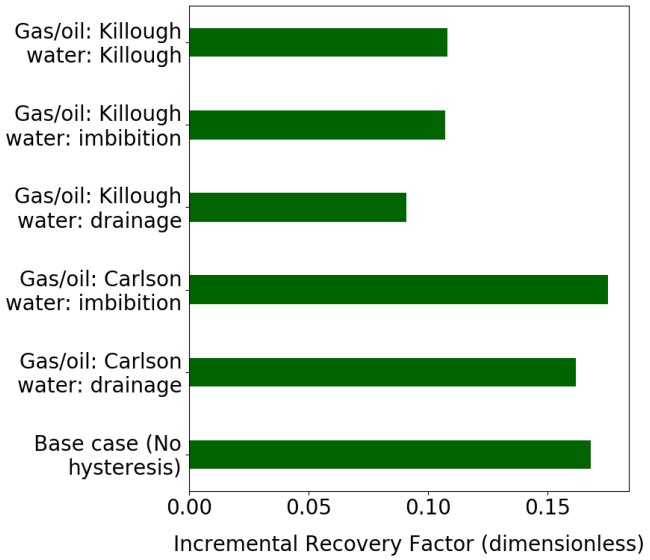

Fig. 15 – Optimal Incremental Recovery Factor (PUNQ-S3)

year of the reservoir life. Figure 17 illustrates the corresponding values of injected pore volume when the WAG injection is started. Similar results can be observed for the PUNQ-S3 model as depicted in Figures 18 and 19. A notable observation is that if no active hysteresis model is used, WAG should start earlier, after 50 months of production for the PUNQ-S3 model compared to 167 months for the SPE-5 model. The results of optimization on both reservoir models suggest that an early WAG implementation could be beneficial.

As previously mentioned, water and gas slug sizes were not optimized directly due to the constraints imposed by the simulator, rather the injection guide rates were optimized. The water and gas slug sizes are functions of the injection guide rates and the constraints, therefore, the slug size values vary throughout the WAG period.

The optimal gas cycle length and the average gas slug size values for the SPE-5 model using all the hysteresis models are shown in Figure 20 and 21, respectively. For both variables, the variation in the optimal value between the active hysteresis cases and the inactive hysteresis case is significant. While using a hysteresis model results in high values of gas slug size (2.2-3.0 MRm^3) and gas cycle length (125-170 days), using the no hysteresis model shows significantly smaller optimal gas cycle and slug size values.

Figures 22 and 23 present the optimal gas cycle lengths and the average gas slug sizes of each injector for the PUNQ-S3 model using all the hysteresis models. The optimal values obtained with no active hysteresis are still substantially different from the active hysteresis cases. However, as shown, even within the active hysteresis cases, there is a significant variation in the optimal values. For instance, in injector 3, the average gas slug size is 0.010 PV (346,446 Rm^3) for case 1 while it is 0.025 PV (877,413 Rm^3) for case 5.

The optimal water cycle lengths and average water slug sizes of the SPE-5 model are shown in Figures 24 and 25. Similar to the results of the gas phase, higher optimal values of water slug sizes and water cycle lengths are obtained in the no hysteresis case.

Figures 26 and 27 demonstrate the optimal water cycle lengths and the average water slug sizes of the PUNQ-S3 model. In contrast to SPE-5 model results, some of the cases with active hysteresis are at the optimum when the water cycle lengths and the water slug sizes are high. This indicates that activating hysteresis does not necessarily result in lower optimal water slug size and lower optimal water cycle length as it was shown in SPE-5 results. However, it is worth mentioning that case 3 consistently favored lower water cycle length values and lower water slug size in all four injectors.

Implementing a sub-optimal WAG injection due to choosing an inappropriate hysteresis model during the WAG design stage would result in a decrease in the ultimate recovery factor. In order to understand

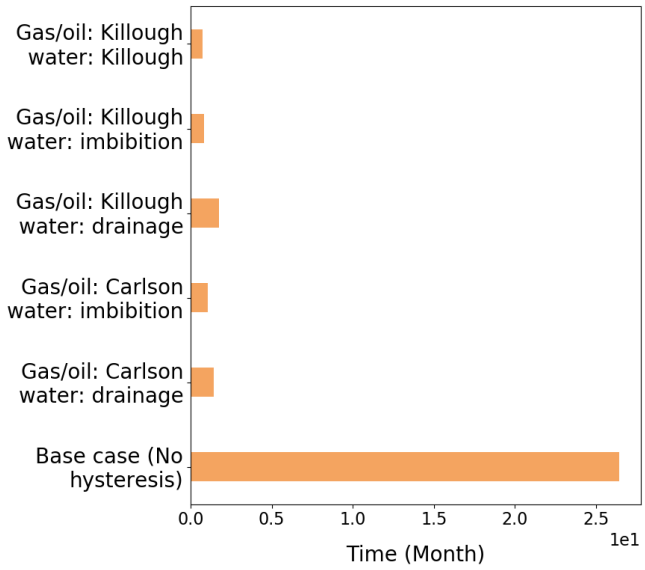

Fig. 16 – Optimal WAG start time (SPE-5)

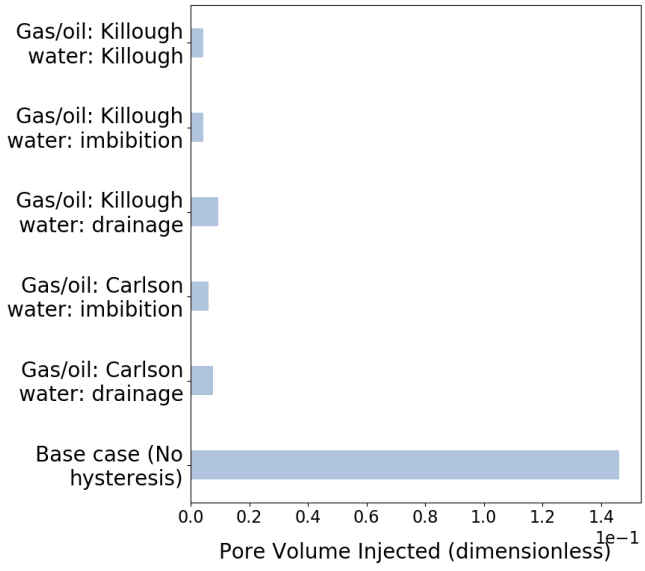

Fig. 17 – Optimal WAG start time in terms of injected pore volume (SPE-5)

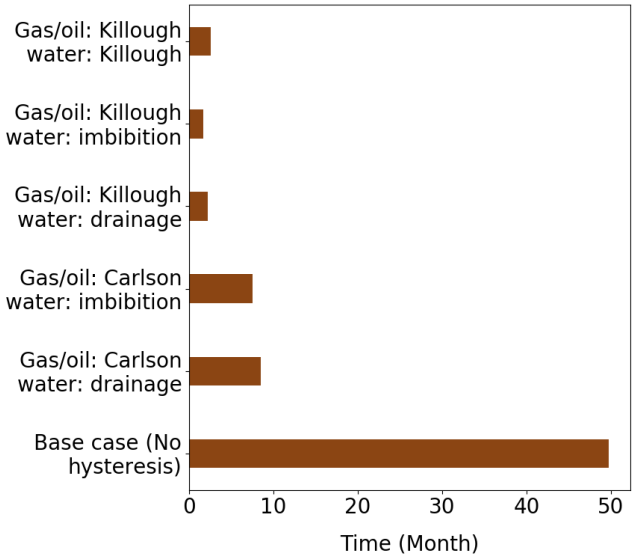

Fig. 18 – Optimal WAG start time (PUNQ-S3)

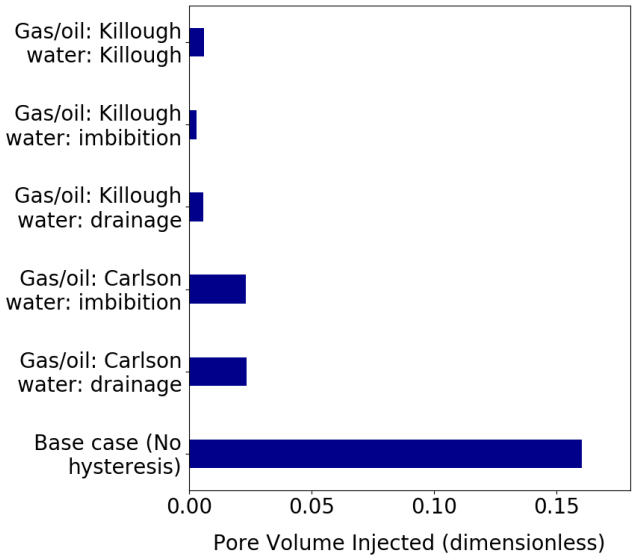

Fig. 19 – Optimal WAG start time in terms of injected pore volume (PUNQ-S3)

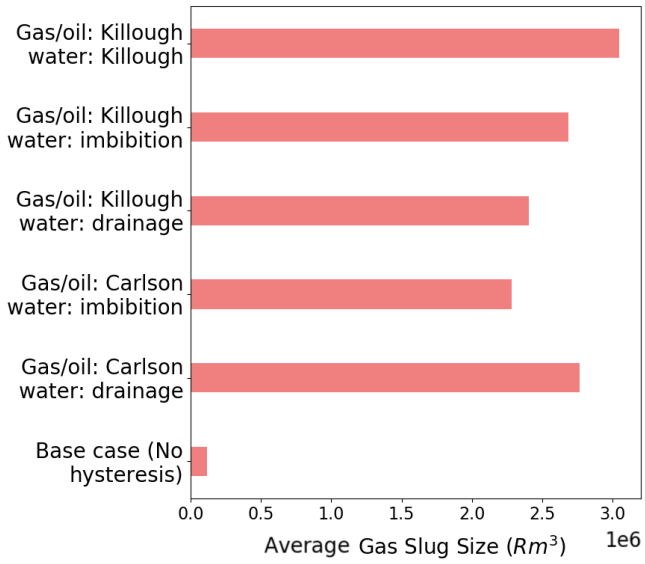

Fig. 20 – Average gas slug size (SPE-5)

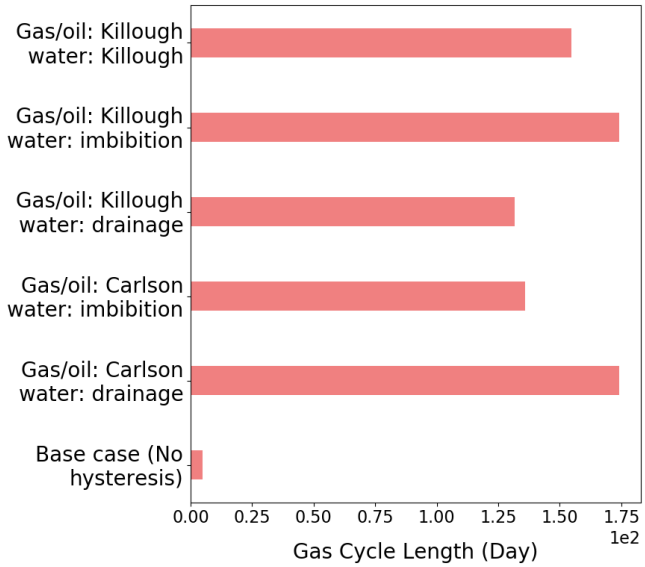

Fig. 21 – Optimal gas cycle length (SPE-5)

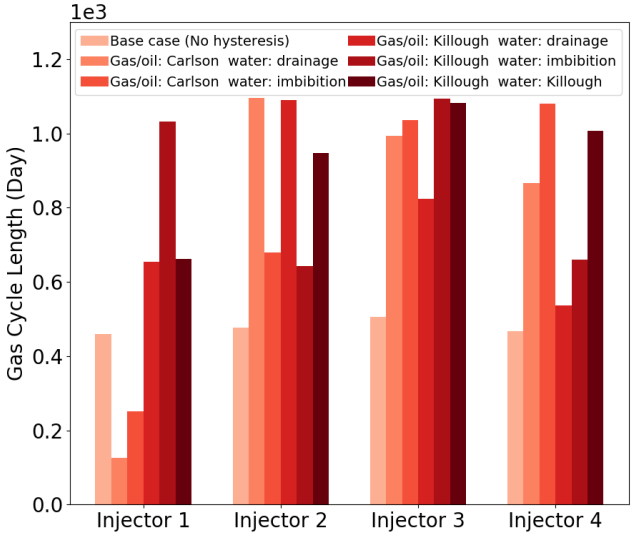

Fig. 22 – Optimal gas cycle length (PUNQ-S3)

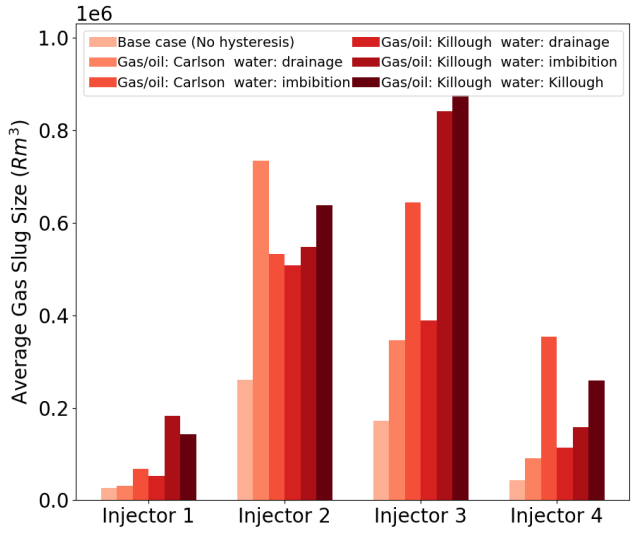

Fig. 23 – Average gas slug size (PUNQ-S3)

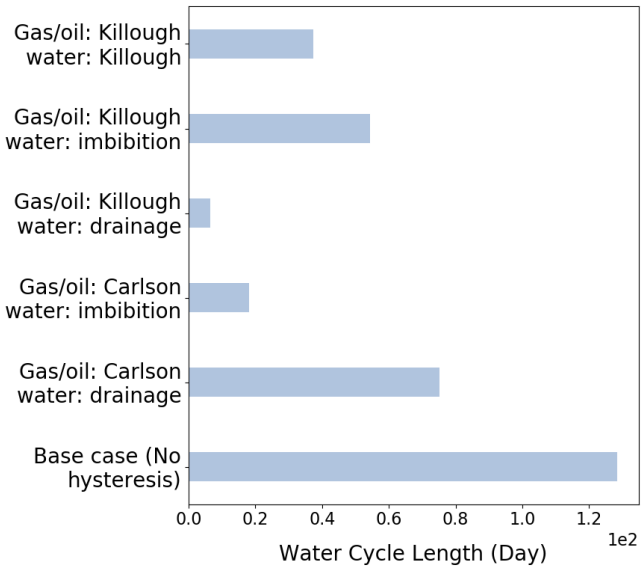

Fig. 24 – Optimal water cycle length (SPE-5)

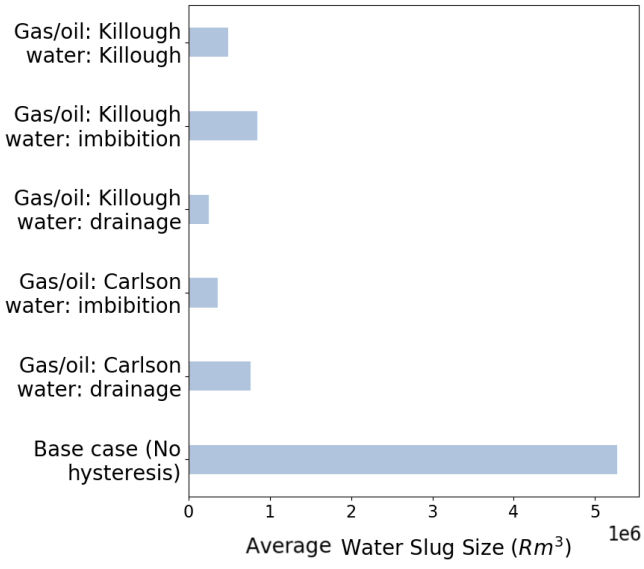

Fig. 25 – Average water slug size (SPE-5)

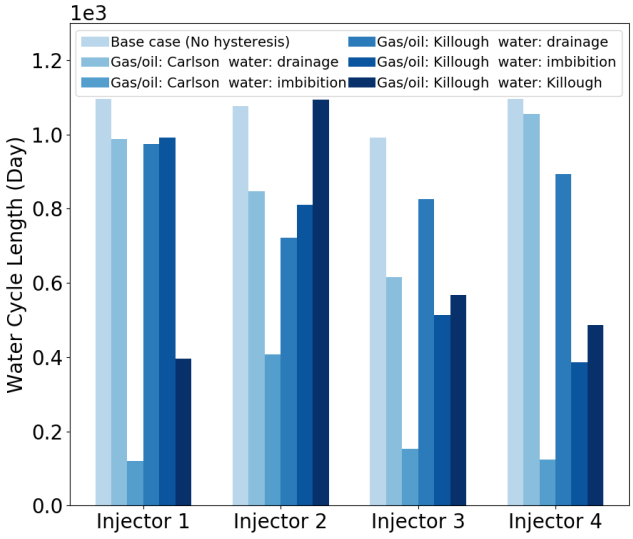

Fig. 26 – Optimal water cycle length (PUNQ-S3)

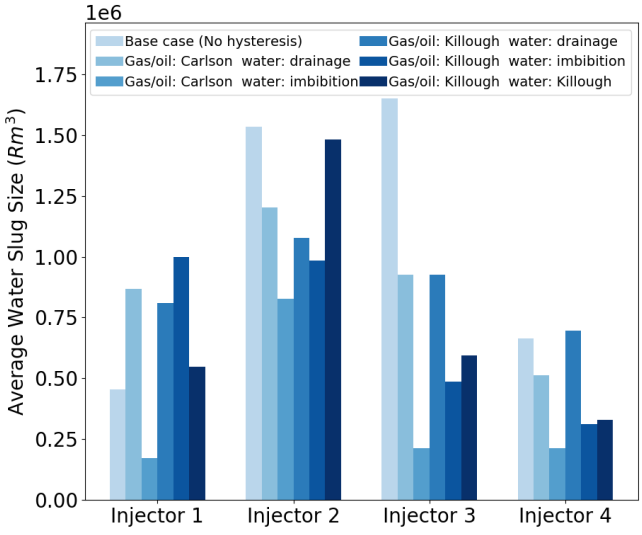

Fig. 27 – Average water slug size (PUNQ-S3)

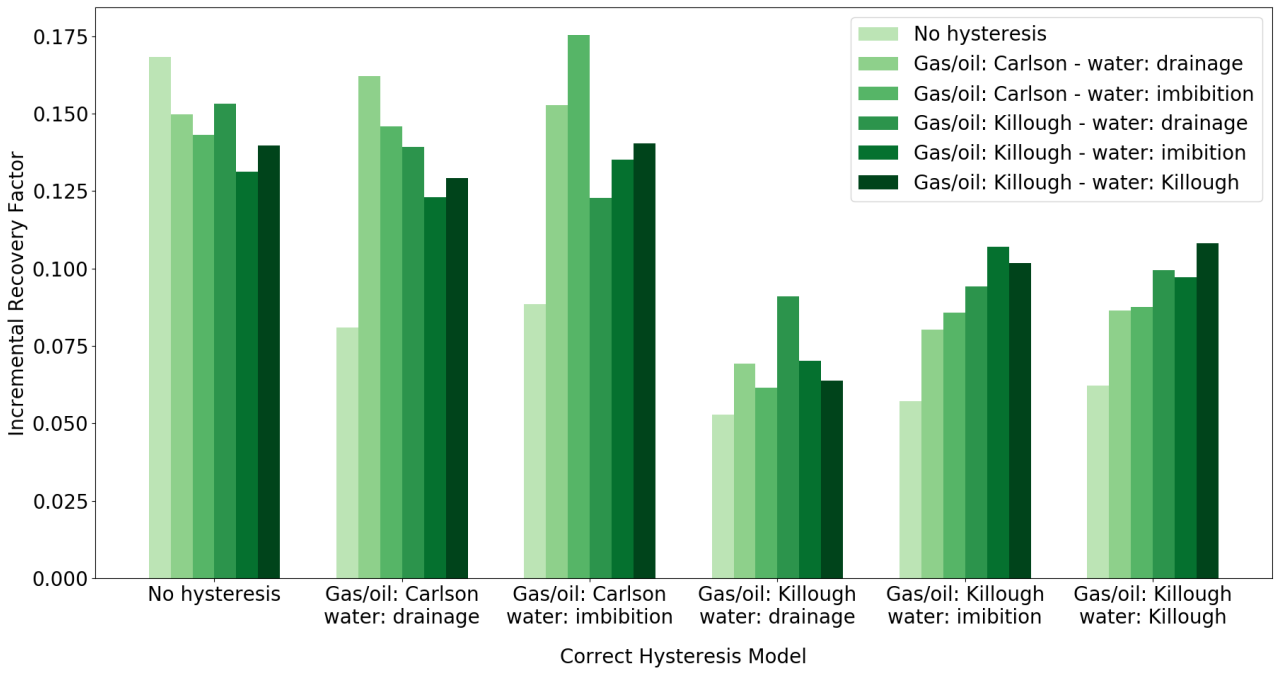

Fig. 28 – Sub optimal design of WAG due to wrong choice of hysteresis model (PUNQ-S3)

the significance of the loss due to a sub-optimal design, for each hysteresis model, we tested the optimal development scenarios that were obtained by optimizing assuming the other hysteresis models. The results are depicted in Figure 28. For instance, assuming the Killough model is used for all phases (case 5) in the WAG injection design, if the hysteresis behavior of the reservoir is closer to the Carlson model (case 1), the suboptimal design of WAG due to the wrong choice of hysteresis model can lead to 3.5% loss in the recovery factor. This indicates that selecting the appropriate hysteresis model is important for a successful WAG injection. In situations where finding the appropriate is not possible due to the lack of data, performing optimization under uncertainty could be a good alternative. The sensitivity to the choice of hysteresis model is greater when the hysteresis behavior of the reservoir is best described by the Carlson model. The loss in recovery due to the wrong choice of the hysteresis model is more pronounced.

Conclusions

- Our sensitivity analysis results show that for both reservoir models under study, the SPE-5 and the PUNQ-S3, the predicted produced oil and produced gas in WAG development are expected to be higher when no hysteresis model is active, i.e. when only the drainage curves are used for the simulation. However, the predicted produced water is expected to be lower in the case of an inactive hysteresis model.
- Our investigation has shown that the optimal recovery factor of WAG process is a function of the chosen hysteresis model. The difference between the highest and lowest values of the optimal recovery factor for various hysteresis cases is 8.4% for the PUNQ-S3 model and it is 4.4% for the SPE-5 model.
- The optimal development scenario (optimal WAG parameters) can be severely affected by hysteresis modeling. Utilizing an inappropriate hysteresis model could result in a sub-optimal WAG design which could lead to a loss in the recovery factor of up to 8%. Therefore, selecting the appropriate hysteresis model during the design process is important. For cases where finding the appropriate

hysteresis model is not practical, the designer may consider stochastic approaches such as performing optimization under uncertainty. This is the subject of ongoing work.

Nomenclature

$a_i =$ lower bound of optimization variable i
$b_i =$ upper bound of optimization variable i
$C =$ Land's trapping parameter
$c_j =$ hysteresis case j
$K_{rnd} =$ non-wetting phase relative permeability from the drainage curve
$K_{rni} =$ non-wetting phase relative permeability from the imbibition curve
$K_{rn} =$ hysteresis dependent relative permeability of the non-wetting phase
$K_{rwd} =$ bounding drainage relative permeability
$K_{rwi} =$ bounding imbibition relative permeability
$K_{rw} =$ wetting phase relative permeability
$P^i_{norm,n} =$ normalized optimal value of parameter P
$P^i_{avg} =$ mean normalized optimal value of parameter P
$P^i_{err} =$ standard deviation of optimal normalized parameter P
$P^0_n =$ parameter optimal value obtained by using the no hysteresis model
$P^i_n =$ parameter optimal value obtained by using hysteresis case i
$Phi_g =$ global best weight
$Phi_p =$ population best weight
$PV =$ pore volume
$RF_{WAG} =$ WAG recovery factor
$RF_W =$ optimal waterflood recovery factor
$S_n =$ non-wetting phase saturation
$S_n =$ wetting phase saturation
$S_{hy} =$ maximum non-wetting phase saturation reached
$S_{ncrd} =$ non-wetting phase critical saturation from the drainage curve
$S_{ncri} =$ non-wetting phase critical saturation from the imbibition curve
$S_{ncrt} =$ non-wetting phase trapped critical saturation
$S_{nmax} =$ maximum saturation
$S_{norm} =$ normalized saturation
$U =$ incremental recovery factor
$x_i =$ optimization variable i

Acknowledgements

The authors would like to thank the Hibernia Management and Development Company (HMDC), Chevron Canada Ltd, Petroleum Research Newfoundland and Labrador (PRNL), the Natural Sciences and Engineering Research Council of Canada (NSERC), the Province of Newfoundland and Labrador, and Mitacs

for financial support. We thank our colleagues in the Hibernia EOR Research Group for their technical support.

References

Bahagio, D. N. T. (2013). Ensemble optimization of CO2 WAG EOR.

Bender, S. and Yilmaz, M. (2014). Full-field simulation and optimization study of mature IWAG injection in a heavy oil carbonate reservoir. In *SPE Improved Oil Recovery Symposium*. Society of Petroleum Engineers (SPE).

Beyer, H.-G. and Schwefel, H.-P. (2002). Evolution strategies – a comprehensive introduction. *Natural Computing*, 1(1):3–52.

Bouzarkouna, Z., Ding, D. Y., and Auger, A. (2012). Well placement optimization with the covariance matrix adaptation evolution strategy and meta-models. *Computational Geosciences*, 16(1):75–92.

Carlson, F. M. (1981). Simulation of relative permeability hysteresis to the nonwetting phase. In *SPE Annual Technical Conference and Exhibition*. Society of Petroleum Engineers (SPE).

Chen, B. and Reynolds, A. C. (2016). Ensemble-based optimization of the water-alternating-gas-injection process. *SPE Journal*, 21(03):0786–0798.

Chen, S., Li, H., Yang, D., and Tontiwachwuthikul, P. (2010). Optimal parametric design for water-alternating-gas (WAG) process in a CO2-miscible flooding reservoir. *Journal of Canadian Petroleum Technology*, 49(10):75–82.

Floris, F. J. T., Bush, M. D., Cuypers, M., Roggero, F., and Syversveen, A.-R. (2001). Methods for quantifying the uncertainty of production forecasts: a comparative study. *Petroleum Geoscience*, 7(S):S87–S96.

Forouzanfar, F., Poquioma, W. E., and Reynolds, A. C. (2015). A covariance matrix adaptation algorithm for simultaneous estimation of optimal placement and control of production and water injection wells. In *SPE Reservoir Simulation Symposium*. Society of Petroleum Engineers (SPE).

Fortin, F. A., De Rainville, F. M., Gardner, M. A., Parizeau, M., and Gagné, C. (2012). DEAP: Evolutionary algorithms made easy. *Journal of Machine Learning Research*, 13:2171–2175.

Ghaderi, S. M., Clarkson, C. R., and Kaviani, D. (2012). Evaluation of recovery performance of miscible displacement and WAG processes in tight oil formations. In *SPE/EAGE European Unconventional Resources Conference and Exhibition*. Society of Petroleum Engineers (SPE).

Guzman, R., Domenico, G., Fayers, F., Aziz, K., and Godi, A. (1994). Three-phase flow in field-scale simulations of gas and WAG injections. In *European Petroleum Conference*. Society of Petroleum Engineers.

Hamzei, A., Zargar, G., Arabjamaloei, R., Ekramzadeh, M. A., and Azad, M. (2011). Comparative study of hysteresis models in immiscible water alternating gas (WAG) process. *Petroleum Science and Technology*, 29(12):1214–1226.

Hoseini, J., Masoudi, R., Mirkalaei, S. M. M., Ataei, A., and Demiral, B. (2011). Investigating the effect of hysteresis modelling on numerical simulation of immiscible WAG injection. In *International Petroleum Technology Conference*. International Petroleum Technology Conference.

Humphries, T. and Haynes, R. (2015). Joint optimization of well placement and control for nonconventional well types. *Journal of Petroleum Science and Engineering*, 126:242–253.

Humphries, T. D., Haynes, R. D., and James, L. A. (2014). Simultaneous and sequential approaches to joint optimization of well placement and control. *Computational Geosciences*, 18(3):433–448.

Jesmani, M., Bellout, M. C., Hanea, R., and Foss, B. (2016). Well placement optimization subject to realistic field development constraints. *Computational Geosciences*, 20(6):1185–1209.

Johns, R., Bermudez, L., and Parakh, H. (2003). WAG optimization for gas floods above the MME. In *Proceedings - SPE Annual Technical Conference and Exhibition*, pages 2679–2690.

Kengessova, A. (2020). Prediction efficiency of immiscible water alternating gas performance by lssvm-pso algorithms.

Kennedy, J. and Eberhart, R. (1995). Particle swarm optimization. In *Proceedings of ICNN'95 - International Conference on Neural Networks*, volume 4, pages 1942–1948 vol.4.

Killough, J. (1976). Reservoir simulation with history-dependent saturation functions. *Society of Petroleum Engineers Journal*, 16(01):37–48.

Killough, J. E. and Kossack, C. A. (1987). Fifth comparative solution project: Evaluation of miscible flood simulators. In *SPE Symposium on Reservoir Simulation*. Society of Petroleum Engineers (SPE).

McKay, M. D., Beckman, R. J., and Conover, W. J. (1979). A comparison of three methods for selecting values of input variables in the analysis of output from a computer code. *Technometrics*, 21(2):239–245.

Mirkalaei, S. M. M., Hoseini, J., Masoudi, R., Ataei, A., Demiral, B., and Karkooti, H. (2011). Investigation of different i-WAG schemes toward optimization of displacement efficiency. In *SPE Enhanced Oil Recovery Conference*. Society of Petroleum Engineers (SPE).

Mohagheghian, E., James, L. A., and Haynes, R. D. (2018). Optimization of hydrocarbon water alternating gas in the Norne field: Application of evolutionary algorithms. *Fuel*, 223:86–98.

Poli, R., Kennedy, J., and Blackwell, T. (2007). Particle swarm optimization. *Swarm Intelligence*, 1(1):33–57.

Schlumberger (2017). *ECLIPSE Reference Manual*.

Spiteri, E. J. and Juanes, R. (2006). Impact of relative permeability hysteresis on the numerical simulation of WAG injection. *Journal of Petroleum Science and Engineering*, 50(2):115 – 139.

Spiteri, E. J., Juanes, R., Blunt, M. J., and Orr, F. M. (2008). A new model of trapping and relative permeability hysteresis for all wettability characteristics. *SPE Journal*, 13(03):277–288.

Vivek, R. and Suresh Kumar, G. (2019). An improved brine-relative permeability model with hysteresis and its significance to sequestrated co2 in a deep saline aquifer. *Environmental Earth Sciences*, 78(5):151.

Wang, X., Haynes, R. D., and Feng, Q. (2016). A multilevel coordinate search algorithm for well placement, control and joint optimization. *Computers and Chemical Engineering*, 95:75–96.

You, J., Ampomah, W., Kutsienyo, E. J., Sun, Q., Balch, R. S., Aggrey, W. N., and Cather, M. (2019). Assessment of Enhanced Oil Recovery and CO2 Storage Capacity Using Machine Learning and Optimization Framework. volume Day 4 Thu, June 06, 2019 of *SPE Europec featured at EAGE Conference and Exhibition*. D041S008R006.

Zhou, D., Yan, M., and Calvin, W. M. (2012). Optimization of a mature CO2 flood - from continuous injection to WAG. In *SPE Improved Oil Recovery Symposium*. Society of Petroleum Engineers (SPE).